Figure S1

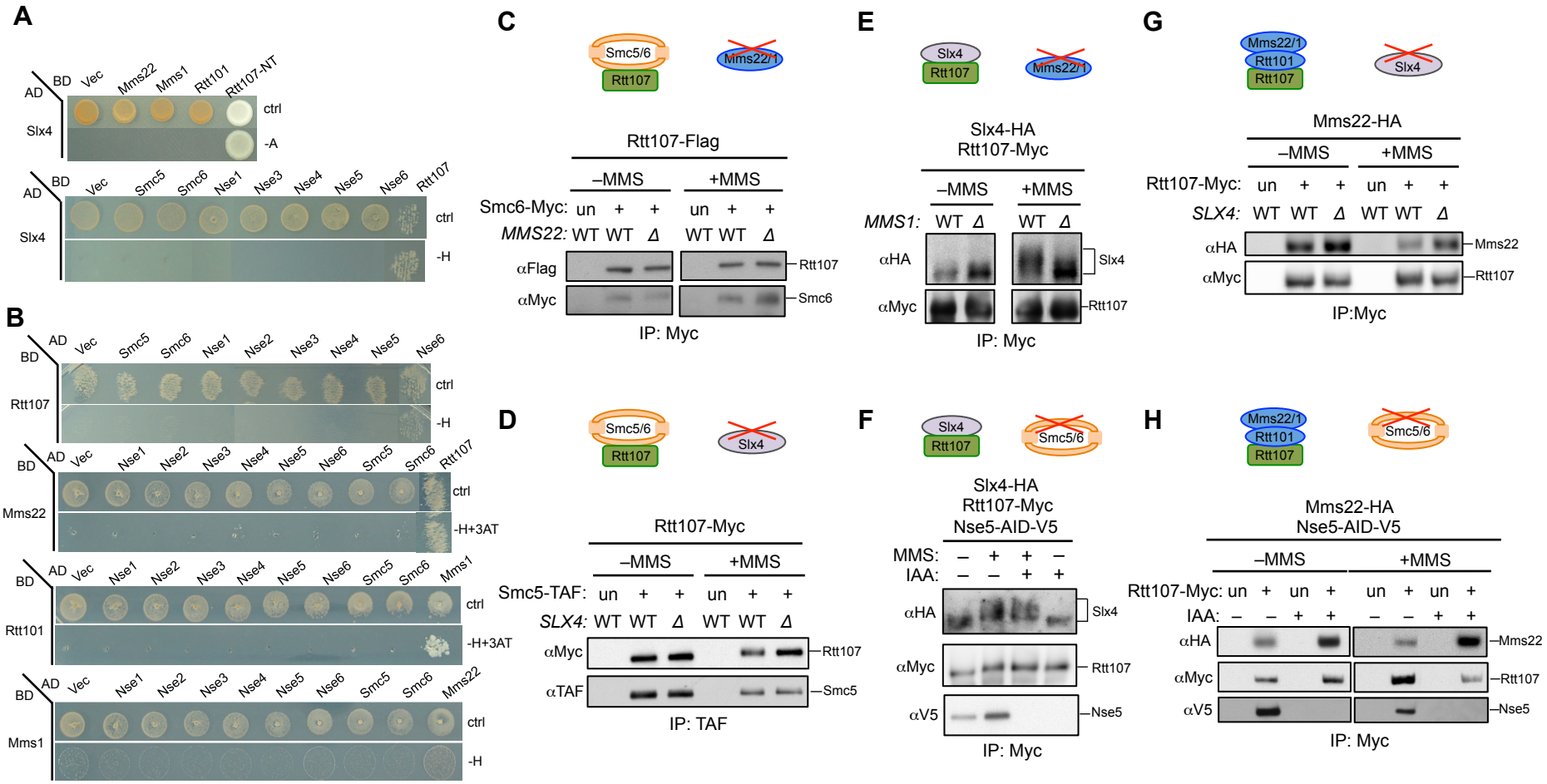
A
AD
BD
Vec
Mms22
Mms1
Rtt101
Rtt107-NT
Slx4
ctrl
-A
Smc5
Smc6
Nse1
Nse3
Nse4
Nse5
Nse6
Rtt107
-H
B
Nse2
-H+3AT
C
Smc5/6
Rtt107
Mms22/1
Rtt107-Flag
–MMS
+MMS
Smc6-Myc:
un
MMS22:
WT
Δ
αFlag
αMyc
Smc6
IP: Myc
D
Slx4
Rtt107-Myc
Smc5-TAF:
SLX4:
αTAF
Smc5
IP: TAF
E
Slx4-HA
Rtt107-Myc
MMS1:
αHA
Slx4
F
Slx4-HA
Rtt107-Myc
Nse5-AID-V5
MMS:
IAA:
αV5
Nse5
G
Mms22/1
Rtt101
Mms22-HA
Rtt107-Myc:
SLX4:
Mms22
IP:Myc
H
Mms22-HA
Nse5-AID-V5

Figure S2

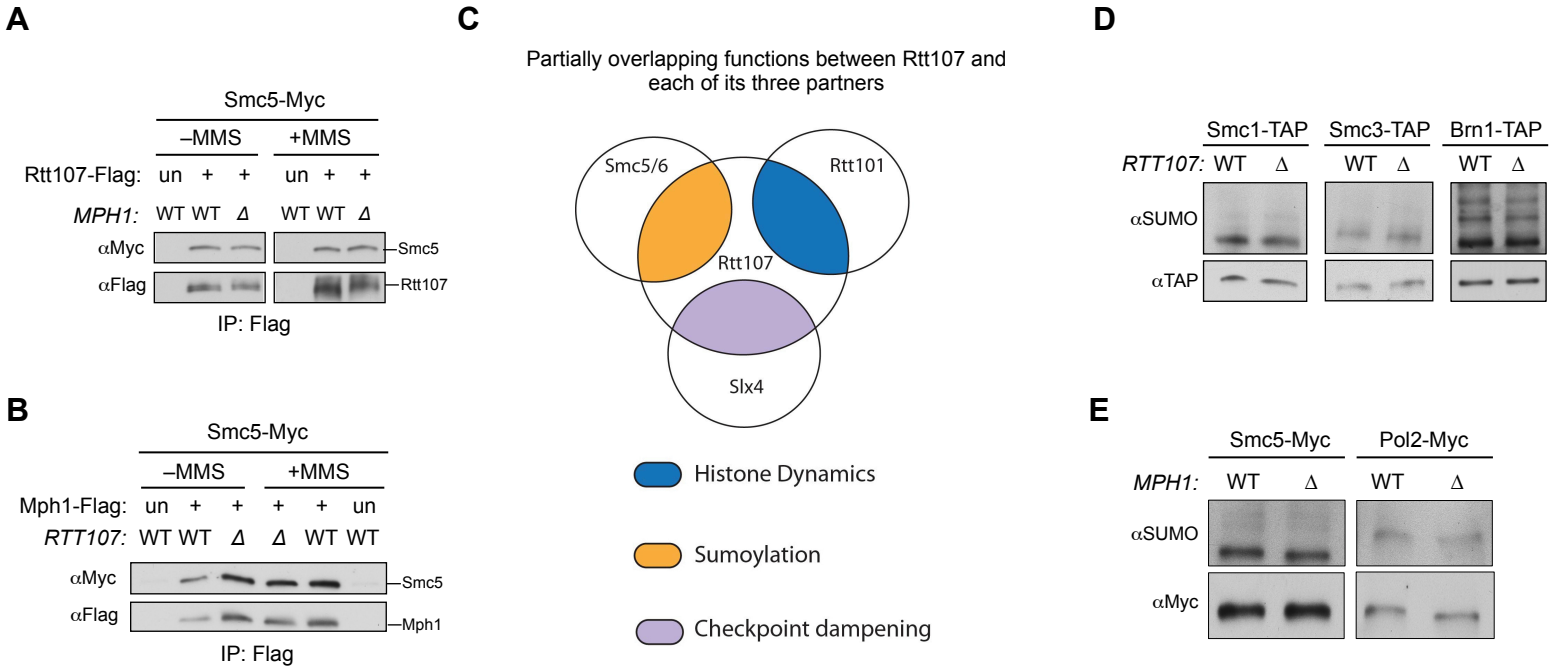
A
Smc5-Myc
–MMS
+MMS
Rtt107-Flag: un + + un + +
MPH1: WT WT Δ WT WT Δ
αMyc
αFlag
Smc5
Rtt107
IP: Flag
B
Smc5-Myc
–MMS
+MMS
Mph1-Flag: un + + + + un
RTT107: WT WT Δ Δ WT WT
αMyc
αFlag
Smc5
Mph1
IP: Flag
C
Partially overlapping functions between Rtt107 and each of its three partners
Smc5/6
Rtt101
Rtt107
Slx4
Histone Dynamics
Sumoylation
Checkpoint dampening
D
Smc1-TAP
Smc3-TAP
Brn1-TAP
RTT107: WT Δ WT Δ WT Δ
αSUMO
αTAP
E
Smc5-Myc
Pol2-Myc
MPH1: WT Δ WT Δ
αSUMO
αMyc

Figure S3

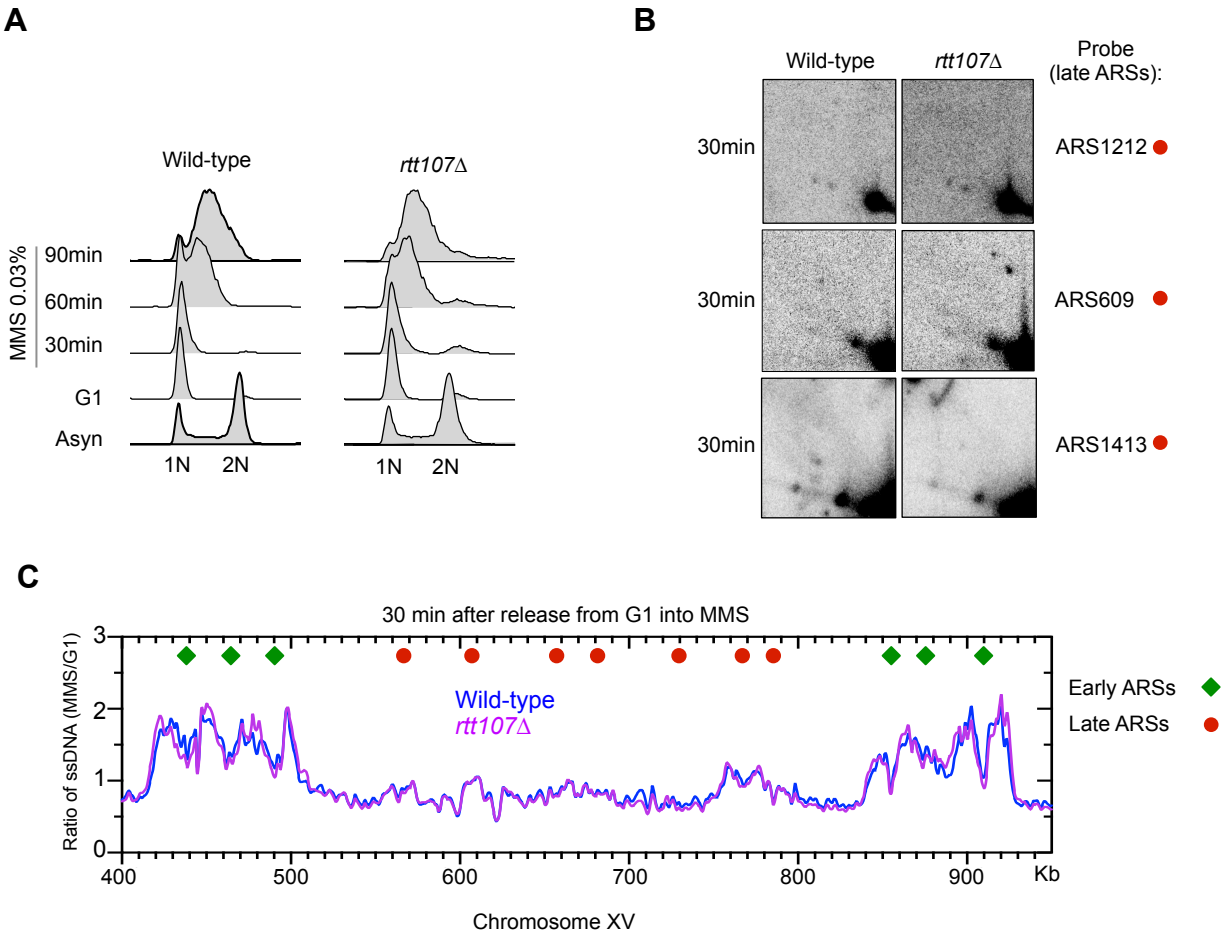
A
Wild-type
rtt107Δ
MMS 0.03%
90min
60min
30min
G1
Asyn
1N
2N
1N
2N
B
Wild-type
rtt107Δ
Probe
(late ARSs):
30min
ARS1212
30min
ARS609
30min
ARS1413
C
30 min after release from G1 into MMS
Ratio of ssDNA (MMS/G1)
Wild-type
rtt107Δ
Early ARSs
Late ARSs
Chromosome XV
Kb

Figure S4

DNA repair pathways required for MMS resistance: representative proteins tested

Base excision repair (BER): Mag1
Nucleotide excision repair (NER): Rad14, Rad23
Post-replicative repair (PRR): Mms2, Rad5, Rad30, Rev3
Homologous recombination (HR): Rad52, Rad1, Csm2

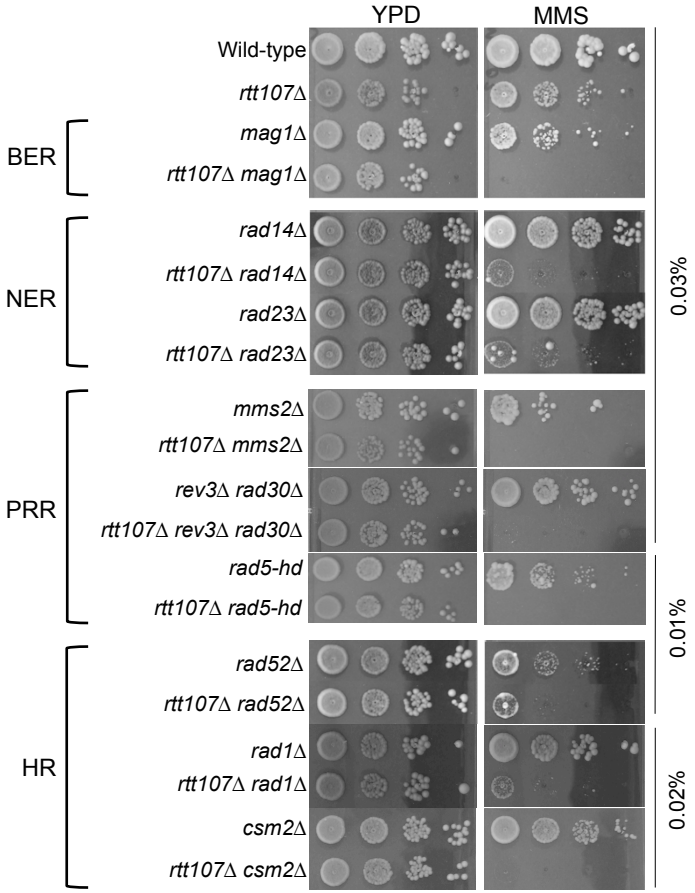

Figure S5

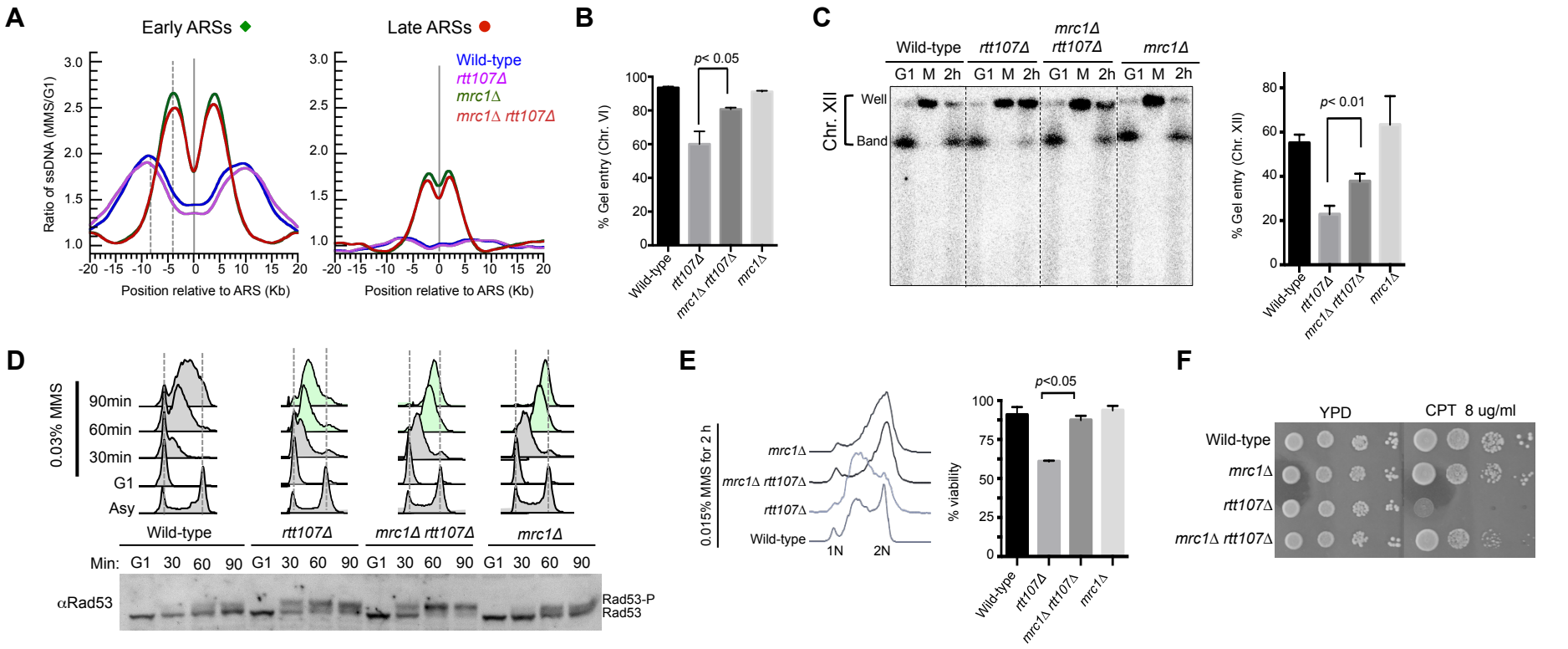
A
Early ARSs
Late ARSs
Wild-type
rtt107Δ
mrc1Δ
mrc1Δ rtt107Δ
Ratio of ssDNA (MMS/G1)
Position relative to ARS (Kb)
B
p< 0.05
% Gel entry (Chr. VI)
Wild-type
rtt107Δ
mrc1Δ rtt107Δ
mrc1Δ
C
Wild-type
rtt107Δ
mrc1Δ rtt107Δ
mrc1Δ
G1 M 2h
Chr. XII
Well
Band
p< 0.01
% Gel entry (Chr. XII)
D
0.03% MMS
90min
60min
30min
G1
Asy
Min: G1 30 60 90
αRad53
Rad53-P
Rad53
E
0.015% MMS for 2 h
1N
2N
p<0.05
% viability
F
YPD
CPT 8 ug/ml
G
YPD
MMS 0.05%
MMS 0.03%
MMS 0.01%
Wild-type
dpb3Δ
rtt107Δ
dpb3Δ rtt107Δ
dpb4Δ
dpb4Δ rtt107Δ
pol2-11
pol2-11 rtt107Δ
(23°C)
pol32Δ
pol32Δ rtt107Δ
ctf4Δ
ctf4Δ rtt107Δ
H
Wild-type
smc6-P4
rtt101Δ
30min
60min
90min
ARS609
ARS1212
ARS1413

Figure S6

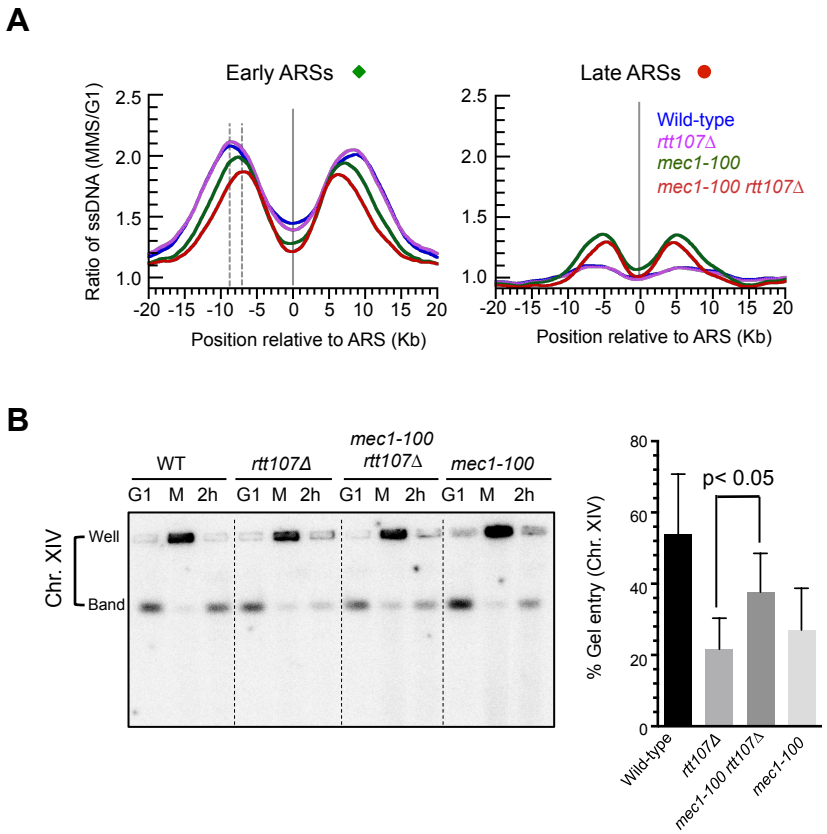
A
Early ARSs
Late ARSs
Ratio of ssDNA (MMS/G1)
Position relative to ARS (Kb)
Wild-type
rtt107Δ
mec1-100
mec1-100 rtt107Δ
B
WT
rtt107Δ
mec1-100 rtt107Δ
mec1-100
G1 M 2h
Chr. XIV
Well
Band
% Gel entry (Chr. XIV)
p< 0.05
C
YPD
CPT 8 ug/ml
Wild-type
mec1-100
rtt107Δ
mec1-100 rtt107Δ

Supplemental Figure Legends

Figure S1 (Related to Figure 1) Rtt107 interacts with each of its partners independently of the other two partners.
(**A-B**) Rtt107 partner proteins associate with Rtt107, but not amongst themselves. (A) Slx4 showed interaction toward Rtt107, but not toward subunits of the Rtt101^{Mms22} or Smc5/6 complexes. Rtt107-NT: 1-660 amino acids. (B) While Rtt107 showed interactions toward specific subunits of the Smc5/6 and the Rtt101^{Mms22} complexes, the subunits of one complex did not show interaction with those of the other. Experiments were performed as in Figure 3G. Control media (ctrl; SC-Trp-Leu) allowed plasmid selection; the SC-Trp-Leu-His (-H) media, the SC-Trp-Leu-His media supplemented with 3AT (-H+3AT), and the SC-Trp-Leu-Ade (-A) media allowed the detection of reporter activation. Note that Y2H constructs of the Smc5/6 complex subunits used here supported previously known interactions (Duan et al., 2009).
(**C-H**) The absence of one Rtt107 partner does not reduce the interaction between Rtt107 with the other two partners. Pair-wise co-IP tests between Rtt107 and its partner proteins were performed in the presence or absence of another Rtt107 partner before and after MMS treatment. The Rtt107-Smc5/6 interaction was sustained when *MMS22* (**C**) or *SLX4* (**D**) was deleted. The Rtt107-Slx4 interaction was not diminished when either Mms1 (**E**) or Nse5 (**F**) was absent. The Rtt107-Mms22 interaction was sustained when Slx4 (**G**) or Nse5 (**H**) was removed. Since the Smc5/6 complex is essential, a degron system was used to acutely deplete the Nse5 subunit of the complex (F, H). In this system, a degron module AID was fused to Nse5 and the degradation was enabled upon the addition of plant hormone Indole-3-Acetic Acid (IAA) in the presence of the degron adapter protein TIR (Nishimura et al., 2009) (Supplemental Experimental Procedures). Nse5 depletion is known to abolish Smc5/6 complex function (Copsey et al., 2013) (Bermudez-Lopez et al., 2015). Note that tested interactions in some cases appeared to increase in the absence of a particular Rtt107 partner.

Figure S2 (Related to Figure 2 and 3) Rtt107 and partner proteins only share a subset of functions.
(**A-B**) Rtt107 and Mph1 are not required for each other's interaction with the Smc5/6 complex. Experiments were performed and results are presented as in Figure S1C.
(**C**) Schematic of the functional relationship between Rtt107 and its three partners. Each protein entity has multiple functions, only some of which overlap.
(**D**) *rtt107*Δ does not affect the sumoylation of subunits of cohesin (Smc1 and Smc3) and condensin (Brn1).
(**E**) *mph1*Δ does not affect the sumoylation of Pol2 or Smc5.
(**D-E**) Experiments were performed as in Figure 1F.

Figure S3 (Related to Figure 4) Examination of replication in *rtt107*Δ cells under MMS conditions.
(**A**) FACS profiles of wild-type and *rtt107*Δ cells for the time course shown in Figure 4.
(**B**) Both wild-type and *rtt107*Δ cells show no replication initiation at the three late origins, ARS1212, ARS609 and ARS1413, at 30 minutes after cells were released from G1 into MMS containing media. Results are part of those shown in Figure 4.
(**C**) Replication fork-associated ssDNA profiles of a segment of Chromosome XV for wild-type and *rtt107*Δ cells. Experimental procedures and labels are identical to those in Figure 5A.

Figure S4 (Related to Figure 4) *rtt107*Δ sensitizes mutants of DNA repair pathways.

The DNA repair pathways and their representative proteins are listed (top). Experiments were performed as in Figure 2B, except that plates were grown for a longer time to better assess the growth of the double mutants.

Figure S5 (Related to Figure 5) *mrc1*Δ increases late origin firing and suppresses several *rtt107*Δ defects, but not Rad53 hyper-activation in *rtt107*Δ cells.

(**A**) Meta-analysis of replication fork-associated ssDNA signals flanking early and late origins. Twenty kilo-bases from either side of early origins (n=97, left) and late origins (n=174, right) were averaged for ssDNA signals and plotted against relative positions of origins. The grey line indicates the midpoint of origins and the dotted line indicates the position of ssDNA peaks flanking the early origins. We estimated the extent of replication fork movement using the positions of signal peaks flanking the origins. On average, replication forks initiated from early origins traveled ~5 kb in *mrc1*Δ cells, approximately half the distance observed in wild-type cells.

(**B-C**) *mrc1*Δ improves chromosomal replication in *rtt107*Δ cells. (**B**) PFGE data on Chromosome VI from two trials were quantified and are presented, related to Figure 5C. % gel entry = signals of the Chromosome VI band in the gel / the signals of this band and those in well.

(**C**) Similar to (**B**) and Figure 5C, except that Chromosome XII was examined.

(**D**) *mrc1*Δ does not correct Rad53 hyper-activation in *rtt107*Δ cells. Asynchronous cells (Asyn) were arrested in G1 and released into media containing 0.03% MMS. Cell cycle progression and Rad53 phosphorylation were examined at the indicated time points by FACS analysis (top) and Western blot (bottom), respectively. FACS analyses showed that while *rtt107*Δ exhibited less DNA synthesis at 60 and 90 min compared with wild-type cells, both *rtt107*Δ *mrc1*Δ and *mrc1*Δ cells similarly exhibited increased levels of DNA content (green). As in Figure 5D, both *rtt107*Δ and *mrc1*Δ *rtt107*Δ cells exhibited increased levels of Rad53 phosphorylation compared with wild-type cells. Note that *mrc1*Δ cells exhibited Rad53 phosphorylation levels similar to those of wild-type cells at high MMS concentrations due to the presence of Rad9 DNA damage checkpoint pathway that activates Rad53.

(**E**) *mrc1*Δ increases the viability of *rtt107*Δ cells after acute MMS treatment. Cell cycle distribution and cell viability were determined and are presented.

(**F**) *mrc1*Δ suppresses *rtt107*Δ cellular sensitivity to CPT. Experiments were performed as in Figure 2B, except CPT was used.

(**G**) Removal or mutation of subunits of replicative polymerases, including Dpb3, Dpb4, Pol2, and Pol32, as well as the replisome subunit Ctf4 does not suppress the MMS sensitivity of *rtt107*Δ cells.

(**H**) *smc6-P4* and *rtt101*Δ mutants are defective in replicating regions far from fired origins. Experiments were done as in Figure 4 and S3A-S3B, except *smc6-P4* (contains a point mutation in Smc6, (Chen et al., 2009) and *rtt101*Δ cells were examined. Shown are representative 2D gel results from at least two independent trials.

Figure S6 (Related to Figure 6) *mec1-100* increases late origin firing and suppresses *rtt107*Δ replication defects and CPT sensitivity.

(**A**) Meta-analysis of replication fork-associated ssDNA signals flanking early and late origins of the indicated strains. Experimental procedures and labels are identical to those in Figure S5A.

(**B**) Similar to Figure 6C, except that Chromosome XIV was examined.

(**C**) Suppression of *rtt107*Δ sensitivity to CPT by *mec1-100.* Experiments were performed as in Figure 2B, except CPT was used.

Supplemental Table (Related to Figure 1-7): Strains and plasmids used in this study

Supplemental Experimental Procedures

ssDNA mapping: Experiments were performed as previously described with some modifications (Feng et al., 2006; Peng et al., 2014). Briefly, early log phase cells were arrested in G1 by the addition of alpha-factor. MMS was then added to the culture as cells were released into S phase. A G1 control sample was collected right before adding MMS and the S phase samples were collected 30 min post-release. Cell pellets were washed with 50 mM EDTA and then embedded in 0.5% low-melt InCert agarose (Lonza) plugs. The embedded cells were spheroplasted and stored in 10 mM Tris-HCl and 1mM EDTA pH 8.0. To label ssDNA, the plugs were first incubated with 50 mM Tris-HCl pH 6.8, 5 mM $MgCl_2$, and 10 mM β-mercaptoethanol, followed by the addition of 50 µl of ssDNA labeling reaction mix. This mix contained 240 µM dATP, 240 µM dCTP, 240 µM dGTP, 120 µM dTTP, 120 µM dUTP labeled with Cy5 (for G1 sample) or Cy3 (for S phase sample), 300 µg/ml random hexamers, and 3,000 units/ml Klenow Fragment (3'-5' exo-) in the same buffer as above. The reaction was incubated at 37°C for 3 hr. To extract chromosomal DNA the plugs were first washed with 10 mM Tris-HCl pH 8.0 and 0.1 mM EDTA at room temperature, then with β-agarase buffer (NEB) on ice. The plugs were melted at 65°C for 10 min and equilibrated at 42°C, followed by the addition of 2 µl β-agarase and incubation at 42°C for 1 hr. The reaction mix was spun at 17,000×g at 4°C for 20 min to remove residual agarose and the chromosomal DNA in the supernatant was sonicated in a Bioruptor (Diagenode Standard Model) to an average size of ~500 bp, followed by purification using the QIAquick PCR Purification Kit (Qiagen).

DNA from an S phase sample and a G1 control sample were co-hybridized onto Agilent G4493A Yeast Whole Genome ChIP-on-Chip 4x44K microarrays. The microarray slides were scanned by an Agilent G2565B scanner and the data extracted by Agilent Feature Extraction software (v 9.5.1). Relative amount of ssDNA at each genomic locus was calculated as the ratio of fluorescence signal from the S phase sample to that from the G1 control sample, followed by Lowess normalization using the statistical software package R (http://cran.r-project.org/). We note that analyzing samples at later time points during S phase such as 60 min after G1 release yielded apparently random distributions of ssDNA as replication forks lose synchrony (data not shown). Meta-analyses were performed as described with some modifications (Smith and Whitehouse, 2012). The 97 early and 174 late origins used for calculations were defined by comparing the Origin database-curated origins (OriDB, http://www.oridb.org, v 2.0.1) to previously reported 105 and 210 Rad53-unchecked (early origins, fire in both wild-type in *rad53* mutant under replication stress) and Rad53-checked origins (late origins, only fire in *rad53* mutant but not wild-type cells under replication stress), respectively (Feng et al. 2006). Origin locations from OriDB were used for calculations. Loci not represented on the microarrays were excluded from calculations. We note that the increased amplitude of ssDNA peaks in *mrc1*Δ compared to wild-type likely reflect more efficient activation of origins. Previous studies have established that the ssDNA mapping method can be used to determine replication fork progression, and has been validated by comparing with more conventional methods (Feng et al., 2009). Importantly and consistent with our findings, *mrc1*Δ and *mec1-100* have been shown to exhibit slow replication fork movement using BrdU ChIP-seq, density transfer, or DNA combing

(Hodgson et al., 2007; Poli et al., 2012; Szyjka et al., 2005; Tourriere et al., 2005; Zhong et al., 2013).

Supplemental References

Bermudez-Lopez, M., Pocino-Merino, I., Sanchez, H., Bueno, A., Guasch, C., Almedawar, S., Bru-Virgili, S., Gari, E., Wyman, C., Reverter, D.*, et al.* (2015). ATPase-dependent control of the Mms21 SUMO ligase during DNA repair. PLoS Biol *13*, e1002089.

Chen, Y.H., Choi, K., Szakal, B., Arenz, J., Duan, X., Ye, H., Branzei, D., and Zhao, X. (2009). Interplay between the Smc5/6 complex and the Mph1 helicase in recombinational repair. Proc Natl Acad Sci U S A *106*, 21252-21257.

Copsey, A., Tang, S., Jordan, P.W., Blitzblau, H.G., Newcombe, S., Chan, A.C., Newnham, L., Li, Z., Gray, S., Herbert, A.D.*, et al.* (2013). Smc5/6 coordinates formation and resolution of joint molecules with chromosome morphology to ensure meiotic divisions. PLoS Genet *9*, e1004071.

Feng, W., Bachant, J., Collingwood, D., Raghuraman, M.K., and Brewer, B.J. (2009). Centromere replication timing determines different forms of genomic instability in Saccharomyces cerevisiae checkpoint mutants during replication stress. Genetics *183*, 1249-1260.

Feng, W., Collingwood, D., Boeck, M.E., Fox, L.A., Alvino, G.M., Fangman, W.L., Raghuraman, M.K., and Brewer, B.J. (2006). Genomic mapping of single-stranded DNA in hydroxyurea-challenged yeasts identifies origins of replication. Nat Cell Biol *8*, 148-155.

Hodgson, B., Calzada, A., and Labib, K. (2007). Mrc1 and Tof1 regulate DNA replication forks in different ways during normal S phase. Mol Biol Cell *18*, 3894-3902.

Nishimura, K., Fukagawa, T., Takisawa, H., Kakimoto, T., and Kanemaki, M. (2009). An auxin-based degron system for the rapid depletion of proteins in nonplant cells. Nat Methods *6*, 917-922.

Peng, J., Raghuraman, M.K., and Feng, W. (2014). Analysis of ssDNA gaps and DSBs in genetically unstable yeast cultures. Methods Mol Biol *1170*, 501-515.

Poli, J., Tsaponina, O., Crabbe, L., Keszthelyi, A., Pantesco, V., Chabes, A., Lengronne, A., and Pasero, P. (2012). dNTP pools determine fork progression and origin usage under replication stress. EMBO J *31*, 883-894.

Smith, D.J., and Whitehouse, I. (2012). Intrinsic coupling of lagging-strand synthesis to chromatin assembly. Nature *483*, 434-438.

Szyjka, S.J., Viggiani, C.J., and Aparicio, O.M. (2005). Mrc1 is required for normal progression of replication forks throughout chromatin in S. cerevisiae. Mol Cell *19*, 691-697.

Tourriere, H., Versini, G., Cordon-Preciado, V., Alabert, C., and Pasero, P. (2005). Mrc1 and Tof1 promote replication fork progression and recovery independently of Rad53. Mol Cell *19*, 699-706.

Zhong, Y., Nellimoottil, T., Peace, J.M., Knott, S.R., Villwock, S.K., Yee, J.M., Jancuska, J.M., Rege, S., Tecklenburg, M., Sclafani, R.A.*, et al.* (2013). The level of origin firing inversely affects the rate of replication fork progression. J Cell Biol *201*, 373-383.